10.1109/ULTSYM.2015.0176

Time Domain Compressive Beamforming: Application to *in-vivo* Echocardiography

Guillaume David*, Jean-luc Robert†, Bo Zhang‡ and Andrew F. Laine*
*Biomedical Engineering Department
Columbia University, New York, NY
Email: gdavid2346@columbia.edu
†Philips Research North America, Cambdrige, MA, Email: jean-luc.robert@philips.com
‡Medisys, Philips Research France, Suresnes, France

***Abstract*—In this contribution we refined our previously introduced time domain compressive beamforming algorithm (t-CBF). Our aim was to make t-CBF less greedy in terms of memory usage to be able to adapt it to real life images. Along the way, we also introduced necessary adjustments to further sparsify our images and make the reconstruction more robust in the presence of speckle. The wavelet transform was implemented in t-CBF in different flavors both in terms of wavelet family and decimated/undecimated algorithm. The cardiac dataset used in this contribution corresponds theoretically to a single diverging wave insonification. Compared to the performance of classic DAS in the same setting, t-CBF yielded better contrast, less sidelobes, and cleaner images.**

I. Introduction

Some applications of ultrasound imaging require a high frame rate to capture the movement of organs with precision. Such an application is echocardiography, where a physician captures images of a beating heart with an ultrasonic scanner in order to detect a pathology related to its movement, or the movement of its valves. Because such movements are quick, a high frame rate is required to capture them [1].

The frame rate of pulse echo imaging is limited by a number of factors including the number of focalized pulses used to compute an image [2]. In the case of cardiac imaging where a typical field-of-view (FOV) can go as deep as 14 cm, the maximum frame rate achievable would be around 30-40 Hz for 2D and around 1 Hz for 3D. The challenge is to decrease the number of focalized pulses necessary per image.

Over the past few years, Compressive Sensing (CS) [3], [4] has gained interest from the beamforming community as it allows the reconstruction of images from less measurements than conventional techniques such as Delay-and-Sum (DAS). Whereas beamforming of medical ultrasound images is typically done in the time domain, CS was previously implemented in the frequency domain [5]. The authors previously developed a time domain compressive beamforming (t-CBF) technique based on expressing beamforming as a matrix operation [6]. Images of bubbles in water at a very high frame rate (about 5 kHz) were demonstrated, as well as hyper-resolution of point scatterers. In this paper, we propose to study how t-CBF performs on images displaying a speckle pattern and in-vivo data using a single diverging wave as the excitation pulse.

II. Methods

A. Overview of the CS tools

CS is a popular technique that uses models and computational power to recover missing information in under-sampled data providing that we can find a space in which that data is sparse enough [7].

a) Sparsity: : A vector is said to be sparse if most of its coefficients are equal to zero [8]. Mathematically, a vector $I \in \mathbb{R}^N$ is said to be S-sparse if all but S of its coefficients are equal to zero.

b) Incoherence: : The acquisition space and the minimization space must be incoherent, that is sufficiently dissimilar [8]. The coherence between two bases Φ and Ψ is usually defined as the maximum absolute value of the cross-correlation between the elements of the two bases [8]. In CS, we are interested in *incoherent* bases or spaces.

We used the tools provided by CS to develop t-CBF, based mainly on l_1-minimization:

$$\min_{I \in \mathbb{R}^N} \|I\|_{l_1} \text{ subject to } \|GI - R\|_{l_2} \leq \epsilon \tag{1}$$

where I is the image, R the raw data from the scanner, G the beamforming matrix as described in [6], and ϵ controls the accuracy of the reconstruction. This problem is commonly known as Basis Pursuit Denoising (BPDN), and we used SPGL1 [9] to solve it efficiently.

B. Matrix beamforming

Consider a homogeneous medium with a single point scatterer. The acquisition process is broken down into several steps. First, the signal is transduced from an electrical impulse to an acoustic pulse: this is modeled by the function $h^i_{\text{sys,Tx}}(t)$, the index i corresponding to the index of the transducer. Then, the acoustic wave propagates in the medium: this is taken into account in the forward propagation function $h_{\text{fwd}}(t_c, \mathbf{r})$. The acoustic wave gets reflected by the scatterer and travels back to the probe: this is the backward propagation $h^i_{\text{bwd}}(t_c, \mathbf{r})$. Finally, the signal is transduced from an acoustic pulse to an electrical impulse: this phenomenon is modeled by $h_{\text{trans}}(t)$. The functions $h^i_{\text{sys,Tx}}(t)$ and $h_{\text{trans}}(t)$ can be temporarily left out of the development as they simply describe the impulse response of the ensemble $\{$scanner+probe$\}$.

Parameter	f_c	bw	λ	N_{elements}	p	c_{sound}	f_s
Value	2.7 MHz	0.6	570 μm	80	$\lambda/2$	1540 m.s^{-1}	32 MHz

TABLE I: Parameters used to build our model G.

This experiment leads to two conclusions: there is a one to one correspondence between a scatterer in the medium and the resulting wavefront the scanner acquires, and if we consider a distribution $I(\mathbf{r})$ of scatterers in the medium, then convolving in time the different terms aforementioned and summing over space gives the raw data R_{ij}, after discretization:

$$R_{ij} = \sum_{k=1}^{N_x} \sum_{l=1}^{N_z} \cdot \left(h_{\text{fwd}}(t_c; k, l) \underset{t_c}{\otimes} h^i_{\text{bwd}}(t_c; k, l) \right)(j) I_{kl} \quad (2)$$

where j is the time index such that t becomes $t_j = j\Delta t$ where $\Delta t = \frac{1}{f_s}$, f_s being the sampling frequency of the system. k and l are the spatial indexes such that the spatial variable $\mathbf{r}$ becomes $\mathbf{r_{kl}} = \begin{pmatrix} x_k \\ z_l \end{pmatrix} = \begin{pmatrix} k\Delta x \\ l\Delta z \end{pmatrix}$ where Δx and Δz are the grid spacing in azimuth and depth respectively. Hence, R_{ij} is the coefficient (i, j) in the raw data matrix R, and I_{kl} is the coefficient (k, l) in the image matrix I. We assume that multiple scattering is negligible which is a classic approximation in medical ultrasound imaging called the BORN approximation [10].

Equation 2 is a tensor product between a bi-dimensional matrix $I = (I_{kl})_{k,l}$ and a four-dimensional tensor $G = (G_{ijkl})_{i,j,k,l}$. Using this notation, we have:

$$G_{ijkl} = \left(h_{\text{fwd}}(t_c; k, l) \underset{t_c}{\otimes} h^i_{\text{bwd}}(t_c; k, l) \right)(j) \quad (3)$$

For a plane wave excitation, we find that:

$$G_{ijkl} = \frac{\delta\left(t_j - \frac{z_l}{c} - \frac{\|\mathbf{r_{kl}} - \mathbf{r_i}\|}{c}\right)}{2\pi\|\mathbf{r_{kl}} - \mathbf{r_i}\|} \quad (4)$$

We added to the model a gaussian bandwidth bw around a central frequency f_c corresponding to the parameters of the probe we used, as shown in table I. The interested reader can refer to [6] for more details.

C. Compressing speckle

The model was used to recover images of point scatterers in [6]. Those images were naturally sparse in the pixel domain. However, most US images are not. They need to be transposed in a domain where they can be well described with few non-zero coefficients. One of the best promoters of sparsity is the wavelet transform [11].

The wavelet transform famously provides us with sparse representations of many types of images. It is widely used in image compression, in the JPEG2000 format for example [11]. It separates details in an image at various scales, from the bulk of the image. As a crude example, let us consider figure 1 (left). This random texture is not sparse. Figure 1 (center) shows its wavelet transform. On figure 1 (right), a reconstruction from the highest 6.2% coefficients of its wavelet transform is shown. The original image and its compressed version are virtually indiscernible.

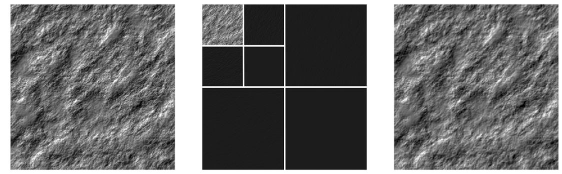

Fig. 1: Left: Original image, random texture. Center: Wavelet transform (HAAR family, level 2 decomposition) of the image. Right: reconstruction of the image from less than 10% of the highest coefficients of the wavelet transform. Energy retained: 99.9%, zeros: 93.8%.

We adapted t-CBF to incorporate the wavelet transform and equation 1 became:

$$\min_{I \in \mathbb{R}^N} \|\Psi I\|_{l_1} \text{ subject to } \|GI - R\|_{l_2} \leq \epsilon \quad (5)$$

where Ψ is the wavelet transform. This problems amounts to minimizing the l_1-norm of the wavelet transform of I under the constraint $\|GI - R\|_{l_2} \leq \epsilon$. We expect the performance of t-CBF to improve in terms of intensity recovered and number of iterations before convergence.

The choice of a good flavor of the wavelet transform will be discussed in the next section.

D. Decreasing the size of G

As stated in [6] the size of G can be prohibitive, even to recover small images. As a result we need to find a way to decrease the size of G and to make sure that it can fit in the RAM in its entirety before using t-CBF in real-life applications. The tool we used to that end is the HILBERT transform.

The HILBERT transform of $f \in \mathbb{R}^{\mathbb{R}}$ is defined by [12]:

$$\mathcal{H}\left\{f(x')\right\}(x) = \frac{1}{\pi} \int_{-\infty}^{+\infty} \frac{f(x')}{x' - x} dx' \quad (6)$$

where the divergence at $x = x'$ is allowed for by taking the CAUCHY principal value of the integral. It is the convolution of $f(x)$ with $-1/\pi x$. Because of the properties of the FOURIER transform of this function, if f is real valued it can be easily proven that the HILBERT transform amounts to discarding the negative frequencies of the signal. This is very advantageous because it allows us to decrease the sampling frequency substantially as explained below.

Consider the spectrum of the real-valued gaussian pulse that we used to model our ultrasonic pulse (figure 2). The sampling frequency is imposed by the difference between the minimal frequency $-f_{\max}$ and the maximal frequency $f_{\max}$. This is SHANNON's theorem [13]. However when we consider the spectrum of the transformed $\mathcal{H}\left\{f(x')\right\}(x)$, we notice that the difference between the minimal and maximal frequencies is much smaller. In fact, it corresponds to the bandwidth of

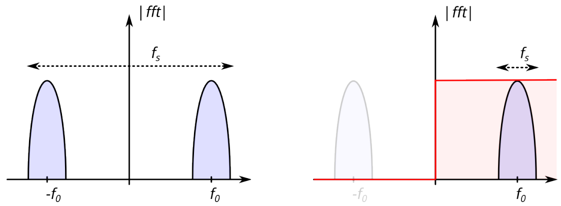

Fig. 2: (left) Spectrum of the gaussian pulse emitted by an ultrasonic probe. The sampling frequency has to be at least $2f_{\max}$. (right) Spectrum of the same signal processed with the HILBERT transform. The negative frequencies are discarded, leading to a complex signal that requires a smaller sampling frequency imposed by its bandwidth.

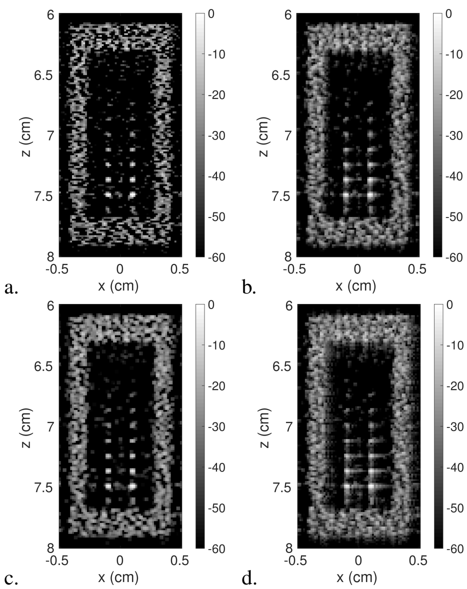

Fig. 3: Numerical phantom recovered with t-CBF: a. without wavelet transform, b. with first order spline wavelets, c. with HAAR wavelets, d. with third order spline wavelets.

the signal. In our case, it allows us to decrease the sampling frequency after HILBERT transform by a factor of 8 to 10.

III. Results

A. Choosing a wavelet family

There are several flavors of the wavelet transform: different wavelet families (HAAR, DAUBECHIE, splines, etc). To determine which family is the most suitable to our problem, we ran t-CBF on a numerical phantom displaying speckle and point scatterers. We focused on compactly supported wavelets and a first order decomposition. The results are presented in figure 3. First, we did not sparsify with wavelets. Then we moved on to first order spline wavelets, HAAR wavelets, and finally third order spline wavelets.

B. Decimated or undecimated wavelets?

The wavelet transform can use decimation at each decomposition level (classic definition) or not. The latter type is

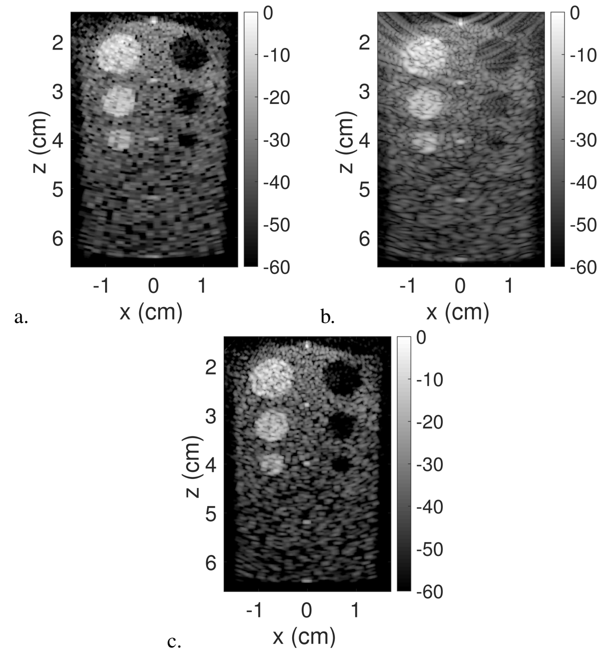

Fig. 4: Numerical phantom recovered with t-CBF: (left) with the classic decimated wavelet transform, (right) with the undecimated wavelet transform.

known as the undecimated wavelet transform. We applied t-CBF to a numerical phantom displaying lesions, cysts, and speckle. We selected HAAR wavelets, decomposed at level 1, and ran t-CBF with the classic decimated wavelet transform first and then the undecimated wavelet transform. The results are presented in figure 4.

C. in-vivo cardiac imaging

The previous improvements allowed us to work with data coming from a commercial US scanner. We used a hardware modified iU22 from Philips (Best, The Netherlands) that allows us to collect the raw data before any kind of processing is applied to the signal.

Because the pulse sequence we use is not standard the scanner's software was also modified to emit diverging waves. The modification had not been approved for use on human subjects at the time this article was written. For that reason, we used a mathematical trick to produce the data we used for reconstruction. Starting from a cardiac dataset we acquired using a classic pulse sequence made of several focalized transmit waves, we applied the virtual transducers principle [14] to calculate the synthetic aperture data [15]. From there, it was straightforward to calculate the response to a diverging wave.

IV. Discussion

A. Choice of a wavelet family

The choice of a wavelet family is inherent to the type of images we need to reconstruct. Different structures in an image can be represented efficiently in different wavelet bases. For

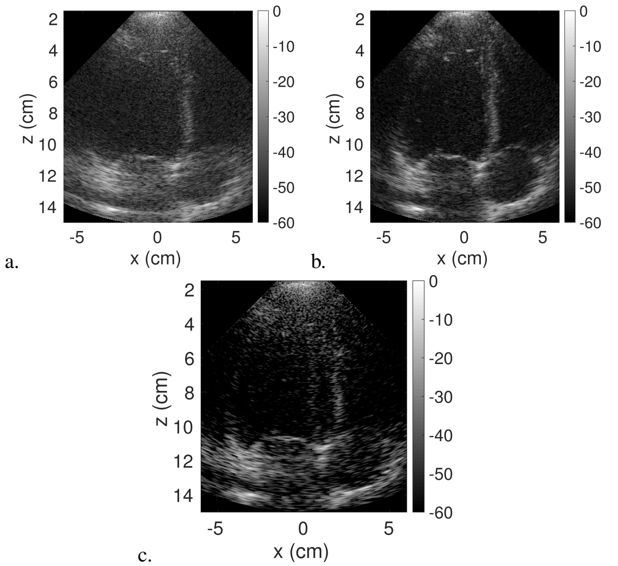

Fig. 5: a. DAS image with 1 diverging transmit wave, b. DAS with 11 diverging transmit waves, and c. t-CBF image with 1 diverging transmit wave.

those reasons, there is probably not an absolute best basis choice to apply t-CBF.

First, section III-A shows that using wavelets helps improve the aspect of the speckle pattern. On figure 3a. we can see that the speckle has a lot of zero-valued pixels and its texture is off. Figures 3b., c., and d. have a smoother speckle pattern that looks more similar to what sonographers are accustomed to.

Then, the resolution seems to be affected by the size of the support of the wavelet basis. More compact supports lead to better resolution: the more compact HAAR wavelets used in figure 3c. lead to better resolution of the point scatterers.

For those reasons, we decided to use HAAR wavelets for the remainder of this work.

B. To decimate or not to decimate?

Decimation speeds up minimization. Undecimation introduces redundancy as well as smoothness which is a desirable property in our case. In III-B a quick comparison of figure 4a. and c. leads to the following observations.

First, the contrast in the cysts and the lesions is better with undecimated wavelets. The lesions and cysts are well-separated from regular tissue.

Then, the resolution of the point scatterers is better when using undecimated wavelets. The image reconstructed using decimated wavelets shows a great reduction of the resolution as we go deeper into the tissue. It even seems to be better than the DAS image in figure 4b.

Finally, figure 4a. displays harsh intensity transitions while figure 4c. is much smoother.

Those results corroborate with similar experiments we conducted on different types of phantoms. It suggests that using undecimated wavelets is beneficial to t-CBF.

C. Cardiac images

The results presented in section III-C are a first glance at how t-CBF can perform in a real-life scenario. The t-CBF image showed in figure 5c. is much cleaner than the DAS images. It allows us to locate structures that are not easily discernible on the DAS images, such as the left ventricular wall. The other structures are preserved and clear. Those results are very encouraging and the next step is to now perform the acquisition with a diverging transmit wave directly.

V. CONCLUSION

We demonstrated that t-CBF could be used on a cardiac dataset. First, we proposed a way to sparsify the image, making the recovery of speckle patterns by t-CBF more robust. We studied a few wavelet families and selected the most relevant. Then, we investigated the advantages and drawbacks of using a decimated or undecimated wavelet transform. Finally we used the HILBERT transform on our dataset as well as to calculate the matrix G in order to decrease its size and make t-CBF applicable to real life images.

REFERENCES

[1] H. Geyer, G. Caracciolo, H. Abe, S. Wilansky, S. Carerj, F. Gentile, H.-J. Nesser, B. Khandheria, J. Narula, and P. P. Sengupta, “Assessment of myocardial mechanics using speckle tracking echocardiography: Fundamentals and clinical applications,” *Journal of the American Society of Echocardiography*, vol. 23, no. 4, pp. 351 – 369, 2010.

[2] B. Angelsen, *Ultrasound Imaging: Waves, Signals, and Signal Processing*. Emantec, 2000.

[3] E. J. Candès, “Compressive sampling,” in *Proceedings of the International Congress of Mathematicians: Madrid, August 22-30, 2006: invited lectures*, pp. 1433–1452, 2006.

[4] R. G. Baraniuk, “Compressive sensing,” *IEEE signal processing magazine*, vol. 24, no. 4, 2007.

[5] M. F. Schiffner and G. Schmitz, “Fast pulse-echo ultrasound imaging employing compressive sensing,” in *Ultrasonics Symposium (IUS), 2011 IEEE International*, pp. 688–691, IEEE, 2011.

[6] G. David, J.-l. Robert, B. Zhang, and A. F. Laine, “Time domain compressive beam forming of ultrasound signals,” *The Journal of the Acoustical Society of America*, vol. 137, no. 5, 2015.

[7] E. Candes and J. Romberg, “Sparsity and incoherence in compressive sampling,” *Inverse problems*, vol. 23, no. 3, p. 969, 2007.

[8] E. J. Candès and M. B. Wakin, “An introduction to compressive sampling,” *Signal Processing Magazine, IEEE*, vol. 25, no. 2, pp. 21–30, 2008.

[9] E. Van Den Berg and M. Friedlander, “SPGL1: A solver for large-scale sparse reconstruction,” *Online: http://www.cs.ubc.ca/labs/scl/spgl1*, 2007.

[10] P. Morse and K. Ingard, *Theoretical acoustics*, pp. 410–414. International series in pure and applied physics, McGraw-Hill, 1968.

[11] B. Usevitch, “A tutorial on modern lossy wavelet image compression: foundations of jpeg 2000,” *Signal Processing Magazine, IEEE*, vol. 18, pp. 22–35, Sep 2001.

[12] R. Bracewell, *The Fourier Transform and Its Applications*. Electrical engineering series, McGraw Hill, 2000.

[13] C. Shannon, “Communication in the presence of noise,” *Proceedings of the IEEE*, vol. 86, pp. 447–457, Feb 1998.

[14] J.-L. Robert and M. Fink, “The time-reversal operator with virtual transducers: Application to far-field aberration correction,” *The Journal of the Acoustical Society of America*, vol. 124, no. 6, 2008.

[15] J. A. Jensen, S. I. Nikolov, K. L. Gammelmark, and M. H. Pedersen, “Synthetic aperture ultrasound imaging,” *Ultrasonics*, vol. 44, Supplement, pp. e5 – e15, 2006. Proceedings of Ultrasonics International (UI05) and World Congress on Ultrasonics (WCU).